Stable and Metastable Phase Equilibria of the In-Se System

T. Gödecke, T. Haalboom, and F. Sommer
Max-Planck-Institut für Metallforschung
Seestrasse 92, D-70174 Stuttgart, Germany

(Submitted 7 April 1998; in revised form 17 June 1998)

The In-Se phase diagram was redetermined using DTA, x-ray analysis, optical microscopy, TEM, and scanning electron microscopy. In_9Se_{11} and In_5Se_7 are stable phases at stoichiometric composition and βIn_2Se_3 was observed at 59.6 at.% Se. βIn_2Se_3 decomposes at 198 °C into γIn_2Se_3 and In_5Se_7. Alloy melts between 33 and 54 at.% Se exhibit a strong tendency for undercooling. Between 50 and 60 at.% Se, the InSe, In_6Se_7, or In_2Se_3 phases solidify directly from the undercooled melt, and the formation of In_5Se_7 and In_9Se_{11} is suppressed while applying cooling rates between 2 to 10 K/min. The respective undercooled states and metastable phase equilibria are provided.

1. Introduction

The $CuInSe_2$-based solar-cell technology will be very important in the near future. Therefore, the phase equilibria of the Cu-In-Se ternary system were investigated [97Haa, 98God]. It was found that some compounds of the In-Se system are in equilibrium with $CuInSe_2$ and that more binary compounds in comparison to the assessed In-Se phase diagram of [91Oka] exist. In the composition range between 50 and 60 at.% Se the number, composition, and formation reaction of the compounds were not determined conclusively. The binodal of the two liquid miscibility gaps are furthermore not completely described [89Gla, 96Cha]. The phase transitions in In_2Se_3 have been studied extensively, but the phase stability and transition types are still controversial as described by [91Oka] and [88Man]. Therefore, it is necessary to reexamine in detail the stable phase equilibria of the In-Se system. The undercooling behavior and metastable phase equilibria are also analyzed in the relevant composition range between 30 and 60 at.% Se.

2. Experimental

2.1 Preparation of Alloys

The components In (purity 99.999) and Se (purity 99.999) with a total weight of 0.5 to 1 g were placed in thick-walled silica ampoules under pure argon atmosphere at 8×10^4 Pa due to the high vapor pressure of Se. The spurting of the liquid alloy during induction melting due to the strong exothermic reaction was minimized by careful regulation of the high-frequency furnace. The master alloys were annealed at 950 °C (1 h) in a resistance furnace and subsequently cooled down in a block of corrosion-resistant steel (X5 CrNiSi 25 20) to room temperature. The solidified master alloy and spurted alloy inside the ampoules were combined by shaking of the silica ampoule and then remelted at 950 °C. The ampoules were shortly annealed at 950 °C and then cooled down to room temperature at 2 K/min. The alloys were subsequently annealed at different temperatures, according to their composition and for sufficient times to equilibrate the samples (see section 3).

2.2 Thermal Analysis

Silica ampoules with very thin walls were used for the DTA. The samples of about 0.25 to 0.5 g were sealed under argon atmosphere at 8×10^4 Pa to prevent the evaporation of Se. Copper of 0.3 g was used as the reference sample. Three ampoules were placed in holes of a small block of corrosion resistant steel (X5 CrNiSi 25 20) directly on top of the thermocouples. Several of the ampoules were removed from the block up to ~ 1000 °C and quenched into water. The microstructure of the quenched, annealed, and cooled DTA samples was investigated by metallography. The variation in the microstructure of the quenched and cooled DTA samples was identified and correlated to the thermal effects obtained by DTA. Heating and cooling rates have been varied between 2 and 10 K/min.

2.3 X-Ray Analysis

The observed microstructure of the annealed samples was supported by XRD measurements. The bulk samples were crushed, and the stress was relieved up to 1 d at the temperature of heat treatment. Powder diffraction investigations were carried out with a Enraf-Nonius RF 552 Guinier camera (Delft, Netherlands) using Cu $K\alpha_1$ radiation. The diffraction patterns of the homogeneous phases were used to identify the phase equilibria of the annealed samples.

2.4 Microscopic Analysis

The samples observed using scanning electron microscopy (SEM) and optical microscopy (OM) were ground and polished with diamond paste. The optical micrographs were taken with polarized light from unetched samples. The samples for TEM were mounted by the procedure of [93Str].

3. Experimental Results

3.1 Stable Phase Equilibria

The stable phase equilibria of the In-Se system based on the new results are shown in Fig. 1. In the temperature range be-

tween 400 and 900 °C, the phase diagram contains the monotectic reactions mo_1 at 520 °C and mo_2 at 750 °C and the peritectic reactions p_1 to p_6. The phases that form peritectically are as follows: βIn_2Se_3 (59.6 at.% Se) at p_1 (880 °C), In_5Se_7 (58.3 at.% Se) at p_2 (670 °C), In_9Se_{11} (55.0 at.% Se) at p_3 (660 °C), In_6Se_7 (53.8 at.% Se) at p_4 (650 °C), InSe (50.0 at.% Se) at p_5 (611 °C), and In_4Se_3 (42.8 at.% Se) at p_6 (550 °C). The δIn_2Se_3 phase melts congruently at 891 °C and transforms polymorphically to γIn_2Se_3 at 745 °C. The critical composition and temperature of the miscibility gap of In-rich liquid alloys are 20 at.% Se and 638 °C, respectively. The corresponding values of the miscibility gap of Se-rich liquid alloys are 75 ± 1 at.% Se and 807 ± 3 °C. The monotectic compositions at 33 at.% (mo_1) and 67 at.% Se (mo_2) were obtained by extrapolating the liquidus temperatures. The liquidus temperatures of alloys with more than 80 at.% Se could not be determined due to the high Se vapor pressure. The measured liquidus temperatures are given in Table 1. Figure 2 shows in detail the results based on DTA and microscopic analysis in the composition range between 33 to 61 at.% Se.

Table 1 Measured Liquidus Temperatures of the In-Se System

at% Se	Liquidus temperature (T_L), °C	at% Se	Liquidus temperature (T_L), °C
5	525	59	880
10	593	60	891
20	637	61	888
30	570	62	870
38	542	64	830
42	573	66	790
48	605	68	770
55	724	70	786
56	780	72	800
56.5	810	77.2	802
58	860		

3.2 Discussion

The temperatures of the monotectic reaction mo_1, peritectic reaction p_6, and position of the phases In_4Se_3, InSe, and In_6Se_7 correspond to the recently assessed data of [91Oka]. It was determined that In_6Se_7 decomposes at 650 °C not at 630 °C as evaluated by [91Oka]. Furthermore, the results in the composition range between 50 and 60 at.% Se differ from the assessed phase diagram (see Fig. 1 and 2). In_9Se_{11} and In_5Se_7 are the stable phases at the stoichiometric composition, and βIn_2Se_3 was observed at 59.6 at.% Se. The microstructures shown in Fig. 3 to 9 verify the new phase equilibria as shown in Fig. 2. The microstructure of the alloy $In_{45.5}Se_{54.5}$ equilibrated at 590 °C for 9 days and 640 °C for 2 days then water quenched displays the phases In_6Se_7 and In_9Se_{11} (see Fig. 3). Figures 4 and 5 show the microstructures of the homogeneous phases In_9Se_{11} and In_5Se_7, respectively. The brightness contrast from polarized light in the OM reveals the grain structure. The samples with compositions from 55 to 58.3 at.% Se, which were annealed at 640 °C show a two-phase microstructure (In_9Se_{11} + In_5Se_7 (dark), see Fig. 6). The dark areas in the micrographs (see Fig. 4 to 6) are holes formed by cracks. The structure of In_9Se_{11} may

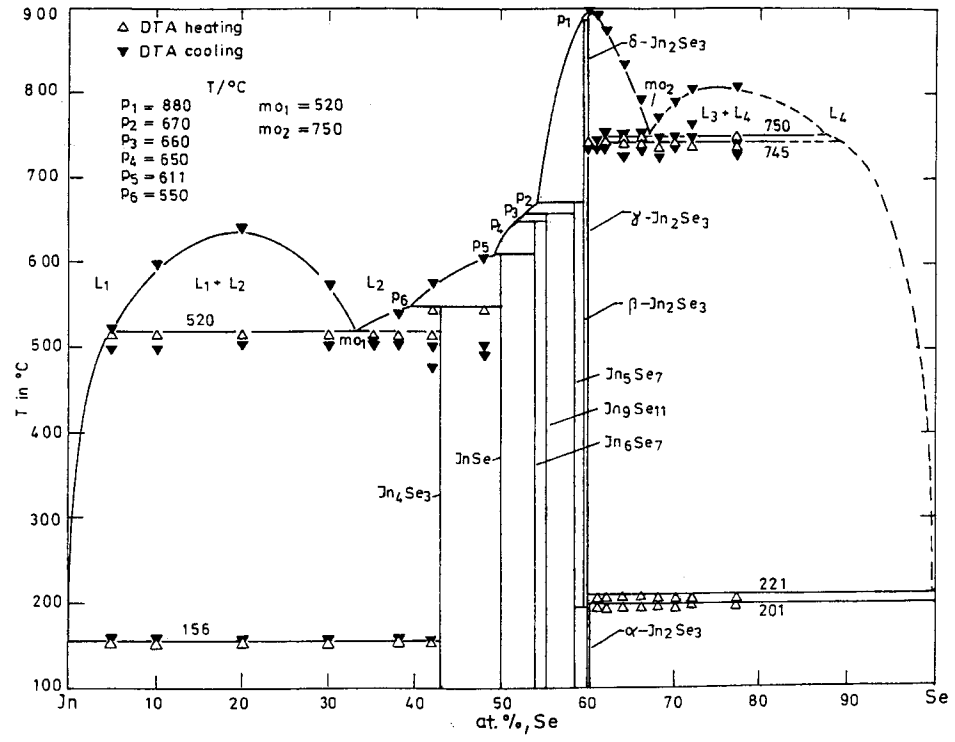

Fig. 1 The In-Se phase diagram.

correspond to the structure of "In_5Se_6" reported by [74Cel]. Six alloys in the composition range from 58 to 60 at.% Se were examined in order to locate the formation of βIn_2Se_3 properly. βIn_2Se_3 is formed at 59.6 at.% Se and 880 °C peritectically from a melt with 59 at.% Se and δIn_2Se_3 with 60 at.% Se. βIn_2Se_3 decomposes at 198 °C to form γIn_2Se_3 (60 at.% Se) and In_5Se_7 (58.3 at.% Se). The microstructure of $In_{40.5}Se_{59.5}$ reveals βIn_2Se_3 (dark) and a few bright spikes of In_5Se_7 (see Fig. 7). In_5Se_7 was easily identified because in polarized light one could observe a color change from bright to dark. γIn_2Se_3 and InSe are brittle and show a laminar structure (see Fig. 8 and 9).

The solid-state phase equilibria given in Fig. 2 were furthermore confirmed by x-ray analysis of the annealed powder of alloys as indicated in Fig. 2. All transformation temperatures given in Fig. 1 and 2 were determined only from effects on heating of properly annealed samples. The liquidus temperatures between p_2 and p_5 were also measured from effects on heating with 2 K/min because liquid alloys in this composition range exhibit strong undercooling (see section 3.3).

The differences between this work and the assessed phase diagram of [91Oka], which is based mainly on the results of [63Sla], [81Ima], and [74Lik], can be ascribed to the different experimental procedures of these authors. The equilibrium phases InSe, In_6Se_7, In_9Se_{11}, In_5Se_7, and βIn_2Se_3 occurred in this work only by an appropriate annealing treatment of the samples. The samples were heat treated at 590 °C (9 days) and for the alloys with more than 53.8 at.% Se additional heat treatment was performed at 640 °C (25 days). These phases were subsequently stepwise cooled down to 190 °C and were annealed again at this temperature for 14 days to prove their stability.

3.3 Undercooling and Metastable States

The undercooled states and metastable phase equilibria of alloys from 30 to 60 at.% Se that were cooled from the liquid state with 2 to 10 K/min are shown in Fig. 10(a). The dotted lines represent the stable phase equilibria. The monotectic reaction mo_1 is undercooled to about 494 °C, and the monotectic

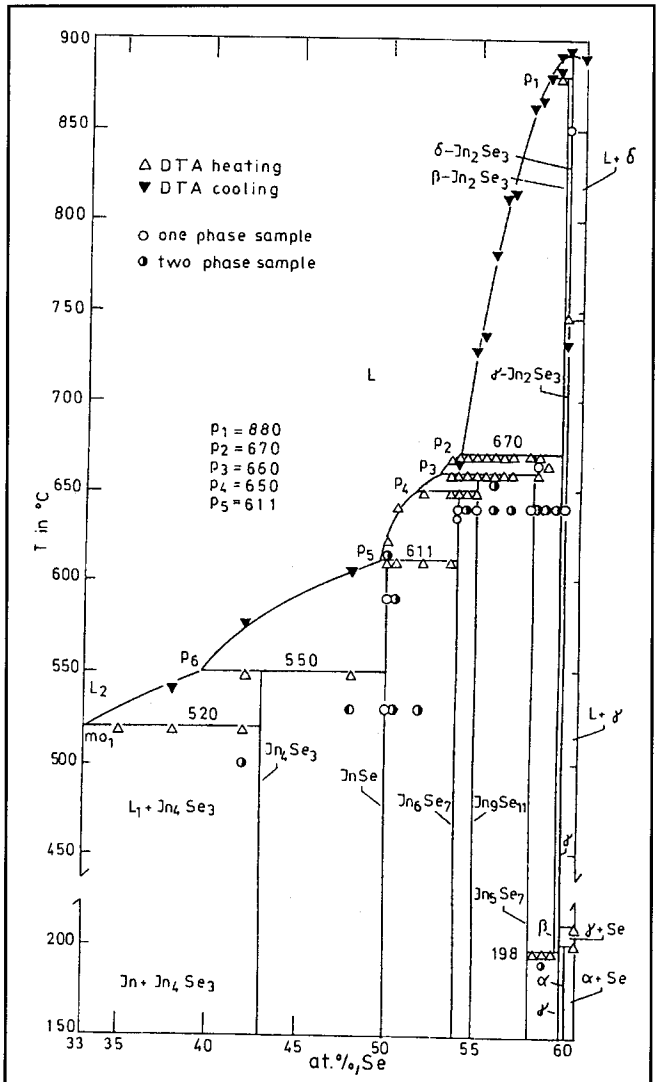

Fig. 2 The In-Se phase diagram in the composition range between 33 and 61 at.% Se.

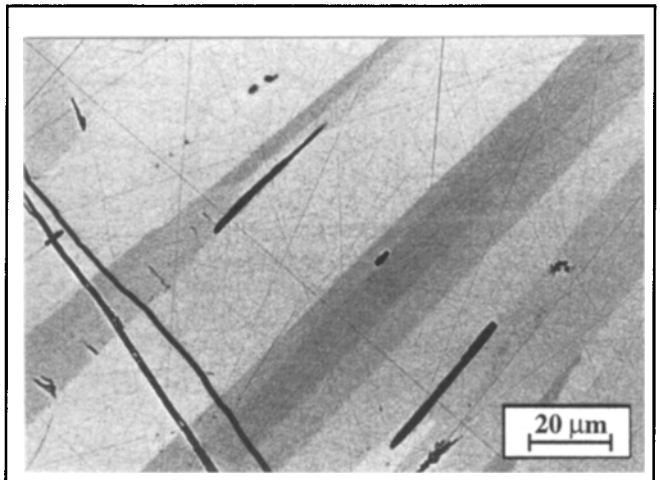

Fig. 3 Microstructure of $In_{45.5}Se_{54.5}$; heat treated at 590 °C/9 d/640 °C/2 d/H_2O; In_6Se_7 + In_9Se_{11} (dark); SEM.

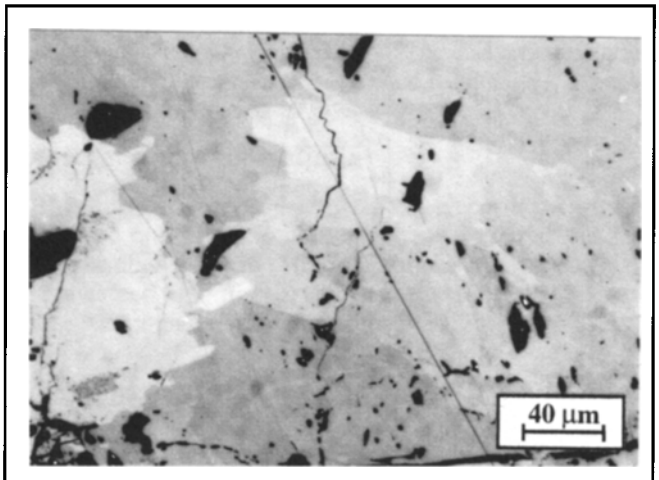

Fig. 4 Microstructure of $In_{45}Se_{55}$; heat treated at 590 °C/9 d/640 °C/2 d/H_2O; In_9Se_{11} homogeneous; OM.

composition is shifted along the metastable extension from mo_1 to mo_1'. The formation of In_4Se_3 is suppressed from 550 °C (p_6) to 504 °C (p_6'). InSe crystallizes directly at 600 °C from the undercooled liquid alloy. A comparison of the XRD pattern of InSe directly after quenching from the liquid state and of the annealed state show distinct differences. The InSe phase crystallized from the undercooled melt is possibly identical with the metastable βInSe phase found by [58Sem]. The liquidus temperatures due to the primary crystallization of δ/βIn_2Se_3 could not be undercooled from 60 at.% Se to p_2. βIn_2Se_3 crystallizes from p_2 to p_2' primarily from the undercooled melt due to nucleation problems of In_5Se_7 and In_9Se_{11} (see Fig. 10b). Alloys with compositions from 56.5 to 59.5 at.% Se exhibit three thermal effects in further cooling between 600 to 592 °C, whereas alloys with a Se composition between 50.5 and 55.5 at.% reveal two additional effects determined from DTA. After cooling, these samples were immediately heated up at 5 K/min. Only two thermal effects were observed at 611 and 650 °C (see Fig. 10b). The undercooled melt (p_2') reacts at nearly constant temperature of 605 °C peritectically with βIn_2Se_3 to form In_6Se_7. The occurrence of a further metastable phase with the stoichiometry In_3Se_4 [65Med] would be not in conflict with the metastable effects shown in Fig. 10(a) and (b), but could not be confirmed from the authors' data. The residual melt decomposes eutectically into metastable βInSe and In_6Se_7 near 590 °C (e_m: L → βInSe + In_6Se_7). The microstructure of $In_{49.5}Se_{50.5}$ reveals clearly regions of eutectic structure between βInSe and In_6Se_7. Figure 11 represents a eutectic (e_m) microstructure formed by bright (In_6Se_7) and gray (βInSe) lamellae. The thermal effects of the heating experiments of the undercooled alloys with compositions from 49 to 54 at.% Se at 611 °C showed that the equilibrium state of InSe has been reached already during heating.

The type and sequence of reactions between 610 and 585 °C during cooling is still uncertain from 56.5 to 59.5 at.% Se. Subsequent heating of undercooled samples did not result in the equilibrium reactions p_3 and p_2. Reactions at p_5 (611 °C) and p_4 (650 °C) have been found. Therefore, it cannot be excluded that during cooling metastable phases such as In_3Se_4 (57.15 at.% Se) are formed rather than the stable phases In_9Se_{11} and In_5Se_7.

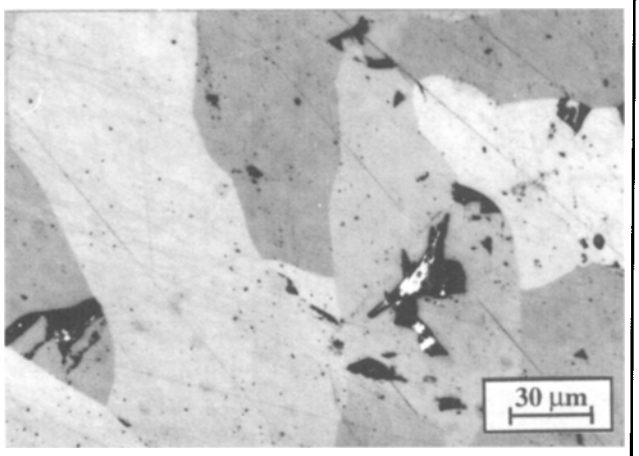

Fig. 5 Microstructure of $In_{42}Se_{58}$; heat treated at 640 °C/25 d/H_2O; In_5Se_7 homogeneous; OM.

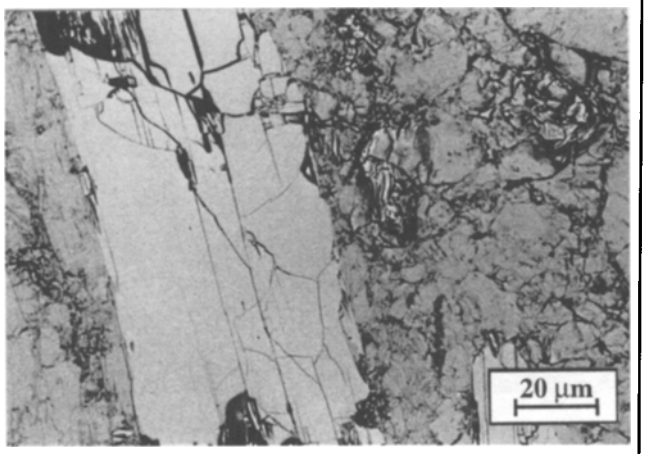

Fig. 6 Microstructure of $In_{44}Se_{56}$; heat treated at 640 °C/25 d/H_2O; In_9Se_{11} + In_5Se_7 (dark); SEM.

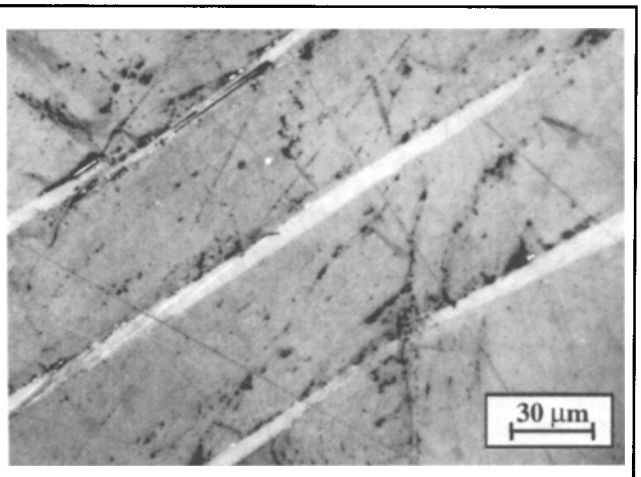

Fig. 7 Microstructure of $In_{40.5}Se_{59.5}$; heat treated at 640 °C/25 d/H_2O; In_5Se_7 (bright) + βIn_2Se_3; OM.

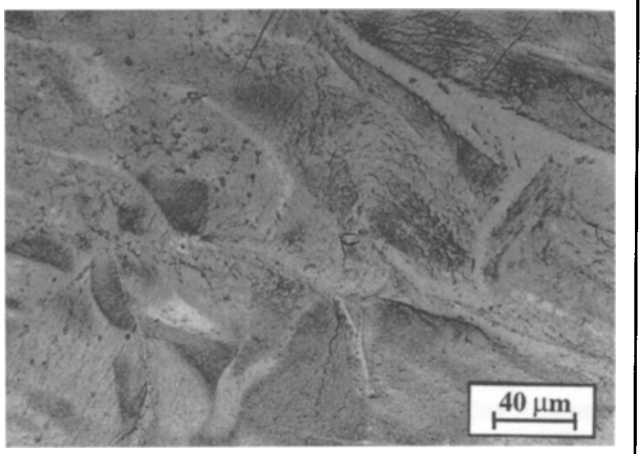

Fig. 8 Microstructure of $In_{40}Se_{60}$; heat treated at 500 °C/4 d/H_2O; γIn_2Se_3 homogeneous; SEM.

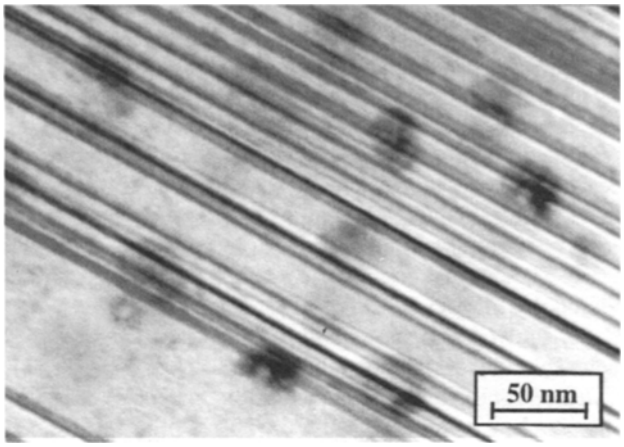

Fig. 9 Microstructure of $In_{50}Se_{50}$; heat treated at 500 °C/5 d/585 °C/24 h/H_2O; InSe homogeneous, TEM.

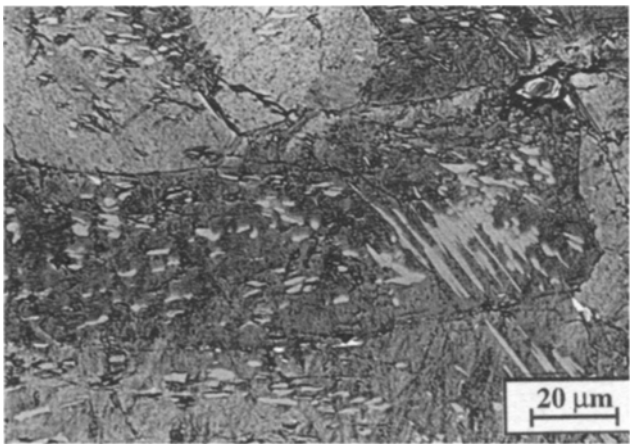

Fig. 11 Microstructure of $In_{49.5}In_{50.5}$; DTA cooling, SEM.

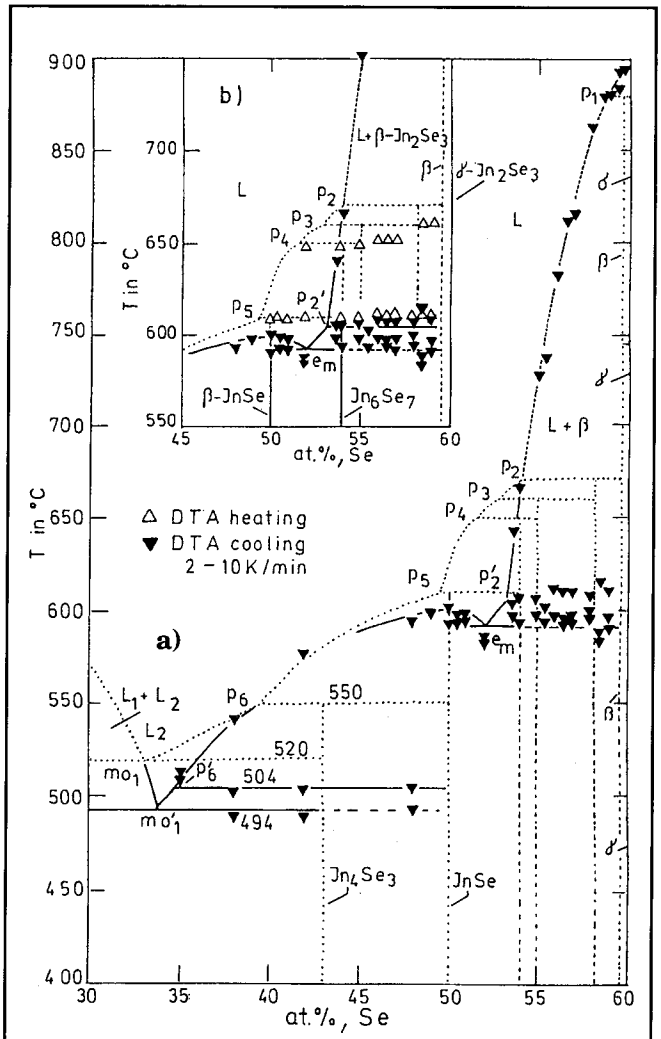

Fig. 10 Undercooled states and metastable phase equilibria obtained by cooling from the liquid state with 2 to 10 K/min.

4. Conclusions

The data from the In-Se system exhibit a great variety of transformations and microstructure formations, which are appreciably influenced by heat treatment and thermal history. Stable and metastable states were distinguished by preparing alloys between 50 and 60 at.% Se at concentration steps of 0.3 to 0.5 at.%. Furthermore a heat treatment was deduced that equilibrates the samples. The reaction temperatures of the stable phases In_9Se_{11} and In_5Se_7 at 660 and 670 °C, respectively, could only be determined from thermograms during heating of equilibrated samples (see Fig. 2). The evaporation of Se during the experiments was excluded. X-ray and microscopic analyses are indispensable in checking the equilibrium state of the samples.

Cited References

58Sem: S.A. Semiletov, *Kristallografiya, 3,* 288-292 (1958).

63Sla: G.K. Slavnova, N.P. Luzhnaya, and Z.S. Medvedeva, *Russ. J. Inorganic Chem., 8,* 78-81 (1963).

65Med: Z.S. Medvedeva and T.N. Guliev, *Zh. Neorg. Khim., 10,* 1520-1524 (1965).

74Cel: J. Celustka and S. Popovic, *J. Phys. Chem. Solids, 35,* 287-289 (1974).

74Lik: A. Likforman and M. Guittard, *Compt. Rend. C, 279,* 33-35 (1974).

81Ima: K. Imai, K. Suzuki, T. Haga, Y. Hasegawa, and Y. Abe, *J. Cryst. Growth, 54,* 501-506 (1981).

88Man: C. Manolikas, *J. Solid-State Chem., 74,* 314-328 (1988).

89Gla: V.M. Glazov, S.G. Kim, and K.B. Nurov, *Izv. Akad. Nauk SSSR Neorg. Mater., 25,* 859-861 (1989).

91Oka: H. Okamoto, in *Phase Diagrams of Indium Alloys and Their Application,* C.E.T. White and H. Okamoto, Ed., ASM International, Materials Park, OH, 242-249 (1991).

93Str: A. Strecker, U. Salzberger, and J. Mayer, *Prakt. Metallogr., 30*(10) 482-495 (1993).

96Cha: C.H. Chang, A. Davydov, B.J. Stanbery, and T.J. Anderson, *The Conference Record of the 25th IEEE Photovoltaic Specialists Conference,* Washington, D.C., Institute of Electrical and Electronics Engineers, 849-852 (1996).

97Haa: T Haalboom., T. Gödecke, F. Ernst, M. Rühle, R. Herberholz, H.W. Schock, C. Beilharz, and K.W. Benz, Int. Conf. on Ternary and Multinary Compounds, ICTMC-11, Salford, U.K., *Inst. Phys. Conf. Ser., 152,* 249-252 (1997).

98God: T. Gödecke, T. Haalboom, F. Ernst, M. Rühle, and F. Sommer, *Z. Metallkd.*